Interner Bericht
DESY F1-72/1
April 1972

— C —

Inclusive Particle Production in pp Interactions at 12 and 24 GeV/c;

I. The Central Region

II. The Proton Fragmentation Region

by

H. J. Mück, M. Schachter, F. Selonke and B. Wessels
University of Bonn

V. Blobel, A. Brandt, G. Drews, H. Fesefeldt,
B. Hellwig, D. Mönkemeyer, H. F. Neumann and P. Söding
DESY and University of Hamburg

G. W. Brandenburg, H. Franz, P. Freund, D. Lüers,
W. Richter, W. Schrankel, B. M. Schwarzschild and P. Weisbach
Max-Planck-Institut für Physik und Astrophysik, München

Submitted to the Proceedings of the International Conference on High Energy Collisions, Oxford, 5-7 April, 1971.

Inclusive Particle Production in pp Interactions at 12 and 24 GeV/c; I. The Central Region

H.J. Mück, M. Schachter, F. Selonke, and B. Wessels, University of Bonn;

V. Blobel, A. Brandt, G. Drews, H. Fesefeldt, B. Hellwig, D. Mönkemeyer, and P. Söding, DESY and University of Hamburg;

G.W. Brandenburg*, H. Franz, P. Freund, D. Lüers, W. Richter, and W. Schrankel, Max-Planck-Institut für Physik und Astrophysik, München

---

* Present address: Stanford Linear Accelerator Center, Stanford, California

One of the problems in high-energy interactions currently much discussed is pionization. It is a crucial feature of inclusive reactions in the multiperipheral model[1], the parton model[2], and the field-theoretical treatment[3] of high-energy collisions. However, comparatively little detailed data from the central or pionization region of inclusive reactions have been published so far[4,5].

In this contribution we present double-differential cross sections for the central region in the reactions $p+p \to \pi^{\pm}$ + anything at incident laboratory momenta of 12 and 24 GeV/c, and compare them with CERN-ISR measurements at higher momenta. We find remarkable regularities when we express these cross sections as functions of y^*, p_T, and s. The use of the c.m. longitudinal rapidity $y^* = \sinh^{-1}(p_{//}^*/(p_T^2 + m^2)^{1/2})$ (where $p_{//}^*$ and p_T are the longitudinal and transverse c.m. momenta), instead of the more conventional variable $x = p_{//}^*/(\sqrt{s}/2)$, is crucial because these regularities in the central region are not evident in the variables x and p_T.

The central (or pionization) region is somewhat arbitrarily defined by $|y^*| < |y_{inc}^*| - \Delta$, where y_{inc}^* is the c.m. rapidity of the incident particles (1.62 at 12 GeV/c and 1.97 at 24 GeV/c) and Δ is a constant of the order of 1. We recall that for asymptotic s the prediction[1-3] for the Lorentz-invariant single-particle distributions in the central region (for unpolarized incident particles) is

$$\frac{d^3\sigma}{d^3\vec{p}/E} \equiv \frac{2E^*}{\pi\sqrt{s}} \frac{d^2\sigma}{dx\,dp_T^2} \equiv \frac{1}{\pi} \frac{d^2\sigma}{dy^*\,dp_T^2} \sim f(p_T), > 0, \qquad (1)$$

with $f(p_T)$ independent of y^* and s (apart perhaps from log s terms), and of the quantum numbers of the incident particles. This behavior corresponds to double-pomeron exchange in a double-peripheral model. If the exchanged quantum numbers are pure C = +1 and I = 0, the functions $f(p_T)$ will be equal for π^+, π^- and π^0.

The data we present come from 130 000 events (54 000 events) observed in the CERN 2 m hydrogen bubble chamber which was exposed to a p beam of 12 GeV/c (24 GeV/c). Events of all topologies were measured on flying-spot digitizers, which also gave ionization information. Using kinematics and ionization it was possible to separately obtain the distributions for pions and protons in the whole backward c.m. hemisphere.[+] Kaons were not distinguished from pions and are therefore included in the distributions given. This is irrelevant in the context of the investigations described here. The overall normalization of the cross sections was checked by comparison of our $\sigma_{tot}(pp)$ with values measured in counter experiments[6]; they agreed within 2 %.

In Figs. 1a and 1b we show the π^- and π^+ inclusive distributions $\pi^{-1}\, d^2\sigma/dy^* dp_T^2$ at $p_T = 0$ and for various regions of p_T, at 12 and 24 GeV/c. The values at $p_T = 0$ have been obtained by a slight extrapolation of our measured complete p_T^2-distributions, by fitting the function $a \cdot \exp(bp_T^2 + cp_T^4)$ to the data in the region $p_T^2 \lesssim 0.3\ (\mathrm{GeV/c})^2$. For the π^+ distribution the 2-prong events (i.e. final states with only two charged particles) were excluded; these events are a background to pionization because the total charge of all pionization products should be zero. We observe the following features:

(1) The distributions tend to become <u>independent of y^*</u> at small $|y^*|$ for all p_T, but particularly so for the smaller values of p_T.[++] (2) The flat regions in y^* show a

---

+ At 24 GeV/c a pion at rest in the c.m. system has a laboratory momentum of 0.49 GeV/c. Therefore the 16 % of π^+/p ambiguities we found occurred only at transverse momenta $p_T > 0.4$ GeV/c. They were resolved on a statistical basis, exploiting the forward/backward symmetry in the c.m. system. The procedure will be described in detail elsewhere.

++ One might suspect that the flatness of the inclusive y^* distributions at small $|y^*|$ could be only a trivial consequence of the symmetry of the pp reaction in the c.m. system, together with the assumption of smoothness of the cross section at $y^* = 0$. That this is not necessarily so can be seen from processes to which pionization does not contribute, like $p+p \to \pi^+ +$ (one charged) + (anything neutral) (2-prongs); or in which pionization is suppressed, like $p+p \to p+\pi^+ + \pi^- + p$ (dominated by baryon resonance production). In these reactions we observe a stronger variation of $d\sigma/dy^*$ at small $|y^*|$; in fact they show a valley at $y^* = 0$.

tendency to become wider with increasing s. (3) The cross sections are s-dependent, i.e. we are not yet in a pure scaling region. (4) The π^+ cross sections are larger than the π^- cross sections, but the π^+/π^- ratio decreases towards 1 with increasing s.

We now compare, in figs. 1c and 1d, our 12 and 24 GeV/c data (represented by the curves) with π^+ and π^- inclusive data measured at the CERN pp Intersecting Storage Rings, at c.m. energies equivalent to incident laboratory momenta between 225 GeV/c and 1500 GeV/c.[7,8] (Note the change in abscissa scale with respect to figs. 1a and 1b.) We show only the data for the smallest available transverse momentum p_T = 0.2 GeV/c; for the larger p_T the comparison comes out similar. To give an idea of how fast the central region is expanding with increasing energy, the values of $|y^*_{inc}|$ are indicated at the bottom of the figures. Since the ISR $\pi^\pm$ data are essentially outside the central region, we also consider the inclusive photon spectra measured[9] at the ISR, which extend to smaller $|y^*|$. From these we calculate, assuming two observed photons per π^o, a value of $\pi^{-1}\, d^2\sigma/dy^* dp_T^2 \approx 44$ mb$(\text{GeV/c})^{-2}$ for inclusive π^o production at p_T = 0.2 GeV/c, y^* = 0 and equivalent laboratory incident momenta of 500 - 1500 GeV/c, as indicated in the figures. It is then seen that the y^* distributions are consistent with an expanding plateau if the numbers of pions of each charge become equal in the central region at large s. A log s increase of the cross section in the region of small $|y^*|$ may persist at ISR energies.

Although the absolute cross section in the central region still depends significantly on s and on the charge of the pion, the form of $f(p_T)$ (see equation (1)) nevertheless shows a remarkable limiting property already in the 12 - 24 GeV/c region. This is seen from figure 2 which shows the logarithmic derivative with respect to p_T^2 (i.e. the "slope") of the p_T^2-distributions, as a function of y^*. As the p_T^2 distributions are not simple exponentials (they change gradually from a steeper slope at small p_T^2 to a flatter one at larger p_T^2), we show the slopes at the two fixed p_T^2 values of 0.1 and 1 $(\text{GeV/c})^2$. Figure 2

gives direct evidence that the form of the transverse momentum distribution is already becoming independent of the pion charge, and very nearly independent of s, at 12-24 GeV/c in the central region. Futhermore at 24 GeV/c the form of the p_T distribution is seen to be independent of y^* up to about $|y^*| = 1$, i.e. the y^* and p_T dependences factorize in a region of $\Delta y^* \approx 2$ around $y^* = 0$.

Another way of looking at the dependence of the transverse momentum distributions on the longitudinal variables, is the study of the x and y^* dependences of the mean transverse momentum $\langle p_T \rangle$. In fig.3 we show $\langle p_T \rangle$ of the π^+ as a function of x and y^*, with the definitions

$$\langle p_T(x) \rangle = \frac{\int p_T \, E^* (d^2\sigma/dx dp_T^2) dp_T^2}{\int E^* (d^2\sigma/dx dp_T^2) dp_T^2} \qquad (2)$$

$$\langle p_T(y^*) \rangle = \frac{\int p_T (d^2\sigma/dy^* dp_T^2) dp_T^2}{\int (d^2\sigma/dy^* dp_T^2) dp_T^2} \, . \qquad (3)$$

The integrations are done at fixed x in (2) and fixed y^* in (3), and extend over the whole kinematic region of p_T^2. In fig. 3a the well-known minimum of $\langle p_T(x) \rangle$ at $x = 0$ ("sea gull effect"[10]) is observed. Figure 3b however demonstrates that $\langle p_T(y^*) \rangle$ does not show significant variation with y^* near the center $x = y^* = 0$. This suggests that the "sea gull effect" at $x \approx 0$ is better looked at as a consequence of (a) the near independence of the form of the p_T distribution of y^* in the central region, together with (b) the rather small extension of this central region at these low incident energies (for fixed x, the smallest p_T^2 correspond to the largest $|y^*|$, and therefore with increasing x it is for the smallest p_T^2 that one is first moving out of the central plateau region).

The distribution of $\langle p_T(y^*) \rangle$ in fig. 3b is affected by the curved kinematic boundary of the $y^* \cdot p_T^2$ space, which allows the largest p_T^2 values only at $y^* = 0$. To reduce its influence we can restrict ourselves, in forming the average $\langle p_T \rangle$, to e.g.

the region $0 < |p_T| < 600$ MeV/c. The distribution of $\langle p_T(y^*) \rangle$ so obtained is also shown in fig. 3b. It is flat in the region $|y^*| \leq 1$, again demonstrating the same y^*-independence in the central region as was observed in fig. 2.

Finally we show in fig. 4 the distribution of the total electric charge emitted per interval of y^*. To calculate the y^* values it was assumed that the particles carrying the charge are either protons or pions, since charged kaons were not distinguished from pions. One finds a large peak from elastic scattering, excitation and fragmentation of the incident protons. Towards the central region this goes over into a very smooth distribution, slightly falling towards $y^* = 0$. Thus one finds less and less of the incident proton's charge re-emitted when one looks into regions that are more and more central, although the number of particles appearing there is very large.

The data presented strongly suggest that some of the features expected for pionization (see equation (1)) already begin to show up in the 12 - 24 GeV/c region. A problem is, of course, the kinematic overlap at these incident momenta between pionization on the one hand, and fragmentation or excitation of the projectile and target protons on the other. Therefore we can not observe pionization here as an isolated phenomenon free of background. However, assuming only proton fragmentation and excitation a convincing explanation for the remarkable regularities of the pion distributions in the central region may be hard to find. From this point of view these regularities would rather seem accidental.

We are indebted to the CERN operation crews of the PS and of the 2m bubble chamber for their excellent cooperation. We wich to particularly thank H.H. Nagel and J. Seyerlein, who have been responsible for the development of our flying-spot digitizers. Finally we thank T.T. Wu for stimulating discussions and suggestions, and K. Böckmann, V.P. Kenney, E. Lohrmann, H.H. Nagel, B. Nellen, N. Schmitz, B.M. Schwarzschild and M.W. Teucher for advice, help, criticism, and active support.

References

1. D. Amati, A. Stanghellini and S. Fubini, Nuovo Cimento 26 (1962) 896;
   K. G. Wilson, Acta Phys. Austr. 17 (1963) 37;
   C. E. De Tar, Phys. Rev. D3 (1971) 128.
2. R. P. Feynman, in High Energy Collisions (Ed. C.N. Yang et al.), New York 1969, p. 237;
   Phys. Rev. Letters 23 (1969) 1415.
3. H. Cheng and T. T. Wu, Phys. Rev. Letters 23 (1969) 1311; 24 (1970) 1456.
4. See e.g. L. Michejda, Nucl. Phys. B35 (1971) 287;
   J. H. Friedman, C. Risk and D. B. Smith, Phys. Rev. Letters 28 (1972) 191;
   L. von Lindern et al., Phys. Rev. Letters 27 (1971) 1745.
5. L. Van Hove, in Proceedings of the Colloquium on Multiparticle Dynamics, Helsinki (1971), p. 227.
6. Particle Data Group, UCRL-20 000 NN (1970).
7. A. Bertin et al., Bologna preprint.
8. L. G. Ratner et al., Phys. Rev. Letters 27 (1971) 86, and to be published.
9. G. Neuhofer et al., Phys. Letters 38B (1972) 51.
10. E.L. Berger, in Proceedings of the Colloquium on Multiparticle Dynamics, Helsinki (1971), p.327.

Figure Captions

1. (a),(b) Invariant inclusive π^- and π^+ differential cross sections $\pi^{-1} d^2\sigma/dy^* dp_T^2$ at 12 and 24 GeV/c, as a function of the c.m. rapidity y^*. The curves connect data points at equal s and p_T, to guide the eye.
(c),(d) Comparison of our 12 and 24 GeV/c data with CERN-ISR data at $p_T = 0.2$ GeV/c and equivalent laboratory momenta between 225 and 1500 GeV/c. The dashed curves are drawn by us to guide the eye.

2. Slopes of the p_T^2 distributions (for constant y^*) as a function of the c.m. rapidity y^*, at two fixed values of p_T^2 for π^- and π^+ from inclusive 12 and 24 GeV/c pp interactions. (The precise definition of the slope is $-(\partial/\partial p_T^2) \ln(d^2\sigma/dy^* dp_T^2)$; it was determined by a fit of the function $a \cdot \exp(bp_T^2 + cp_T^4)$ to the measured $d^2\sigma/dy^* dp_T^2$ in fixed, small intervals of y^* and p_T^2.)

3. Mean values of the transverse momentum $\langle p_T \rangle$ for π^+ from inclusive 12 and 24 GeV/c pp interactions.
(a) $\langle p_T \rangle$ as a function of x;
(b) $\langle p_T \rangle$ averaged over the whole kinematic region of p_T, and $\langle p_T \rangle$ averaged over the region $0 \leq |p_T| \leq 0.6$ GeV/c, as a function of the c.m. rapidity y^*.

4. Distribution of the total electric charge $\Delta Q/\Delta y^*$ of the outgoing particles, as a function of the c.m. rapidity, for 12 and 24 GeV/c pp interactions. The rapidities were calculated under the assumption, that the particles carrying charge are either protons or pions.

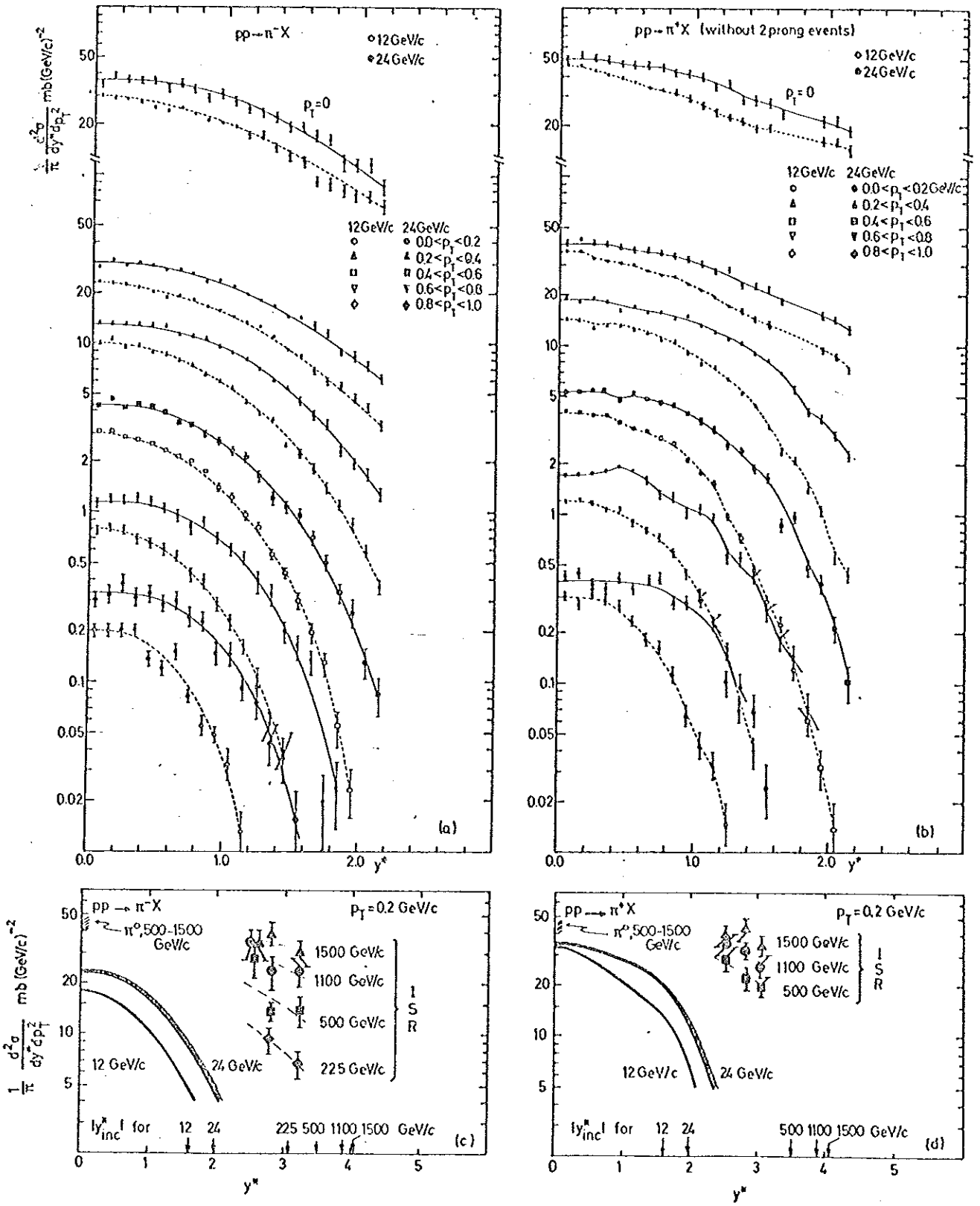
pp→π⁻X
12GeV/c
24GeV/c
p_T=0
12GeV/c 24GeV/c
0.0<p_T<0.2
0.2<p_T<0.4
0.4<p_T<0.6
0.6<p_T<0.8
0.8<p_T<1.0
(a)
pp→π⁺X (without 2prong events)
(b)
pp → π⁻X
P_T = 0.2 GeV/c
π°,500-1500 GeV/c
1500 GeV/c
1100 GeV/c
500 GeV/c
225 GeV/c
ISR
12 GeV/c
24 GeV/c
|y*_inc| for 12 24 225 500 1100 1500 GeV/c
(c)
pp → π⁺X
(d)
y*

Fig. 1

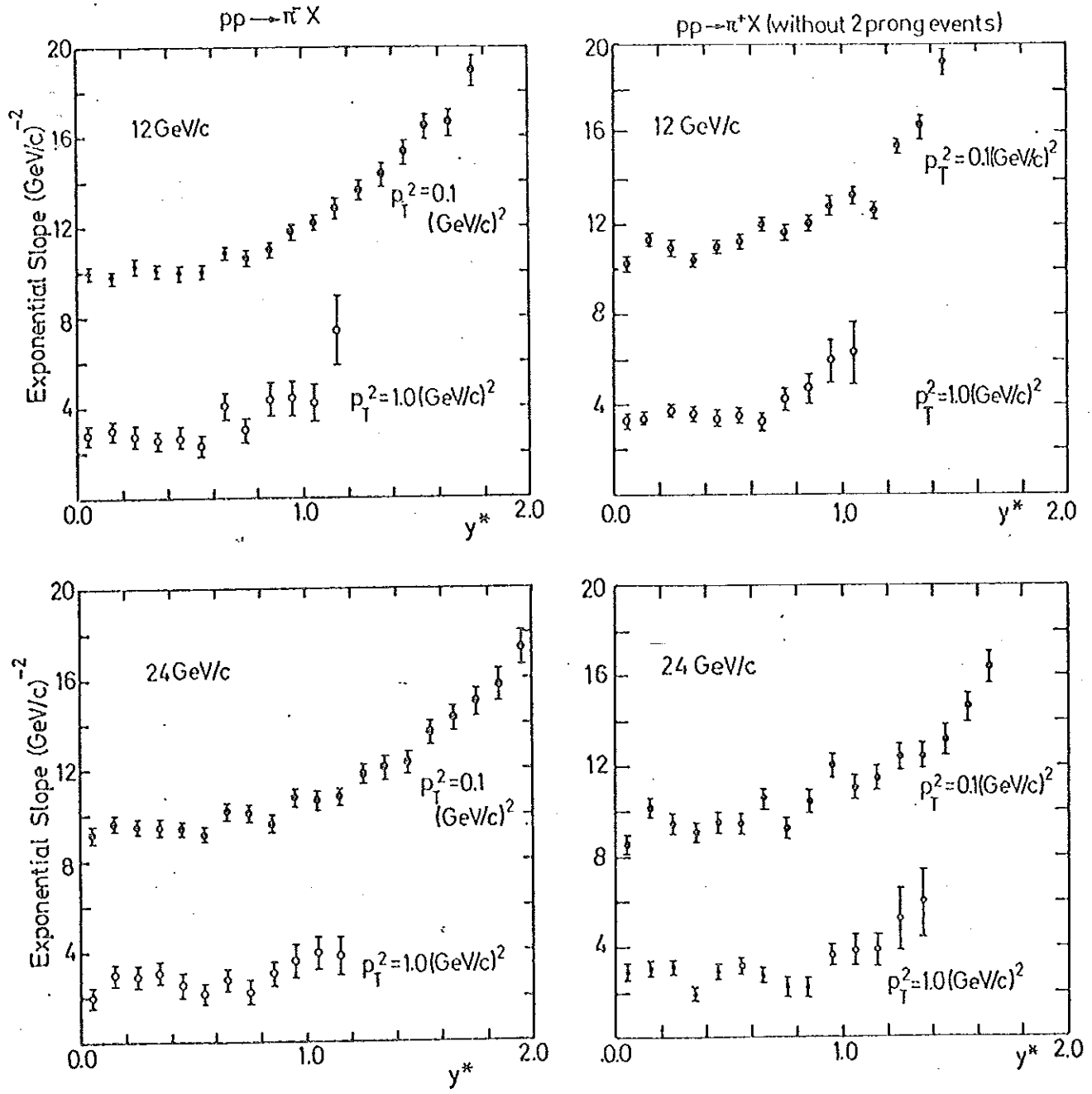
pp → π⁻ X
pp → π⁺X (without 2 prong events)
12 GeV/c
24 GeV/c
p_T^2 = 0.1 (GeV/c)²
p_T^2 = 1.0 (GeV/c)²
Exponential Slope (GeV/c)⁻²
y*
0.0
1.0
2.0
4
8
12
16
20

Fig. 2

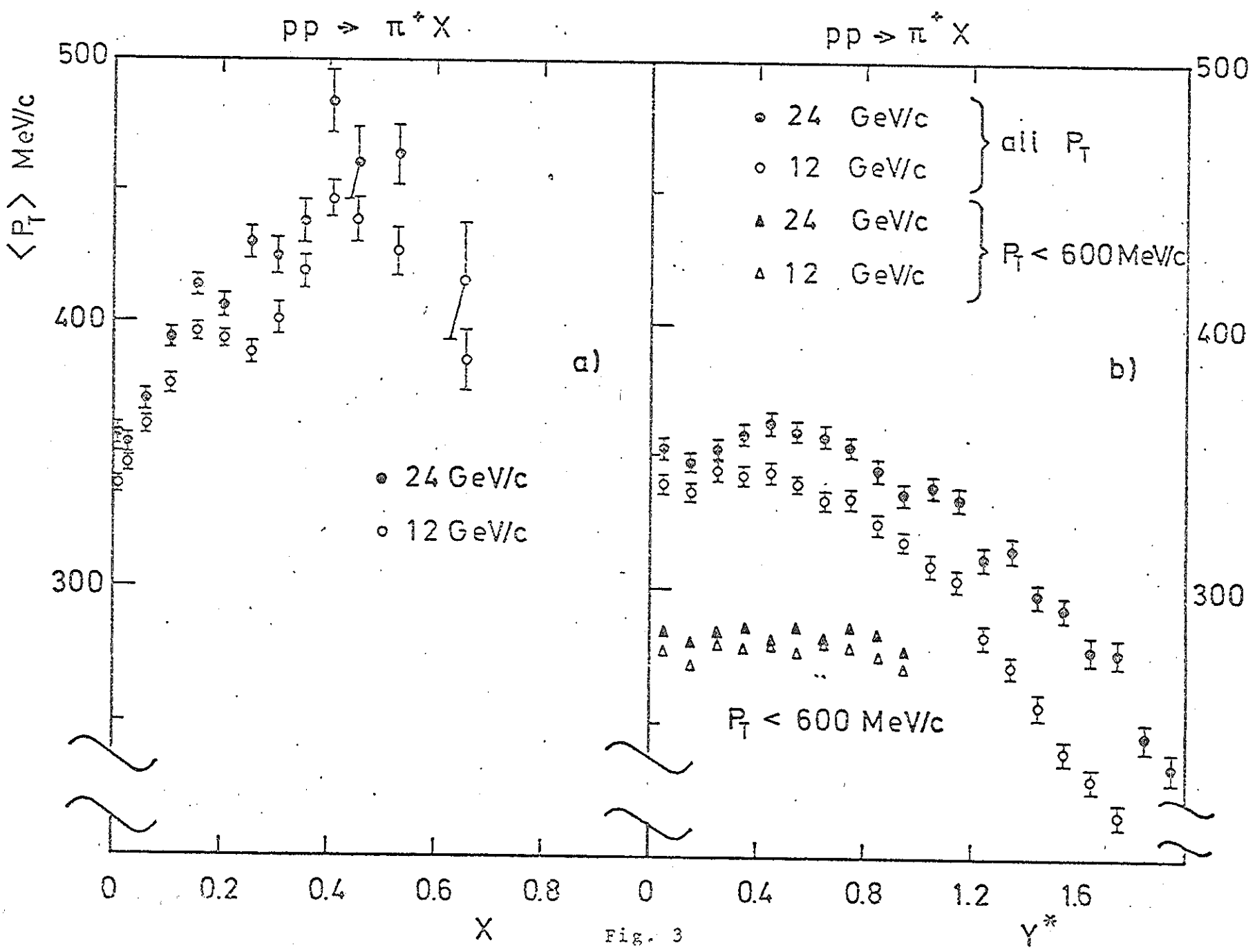
pp → π⁺X
pp → π⁺X
⟨P_T⟩ MeV/c
500
400
300
a)
b)
24 GeV/c
12 GeV/c
all P_T
24 GeV/c
12 GeV/c
P_T < 600 MeV/c
P_T < 600 MeV/c
0
0.2
0.4
0.6
0.8
X
0
0.4
0.8
1.2
1.6
Y*

Fig. 3

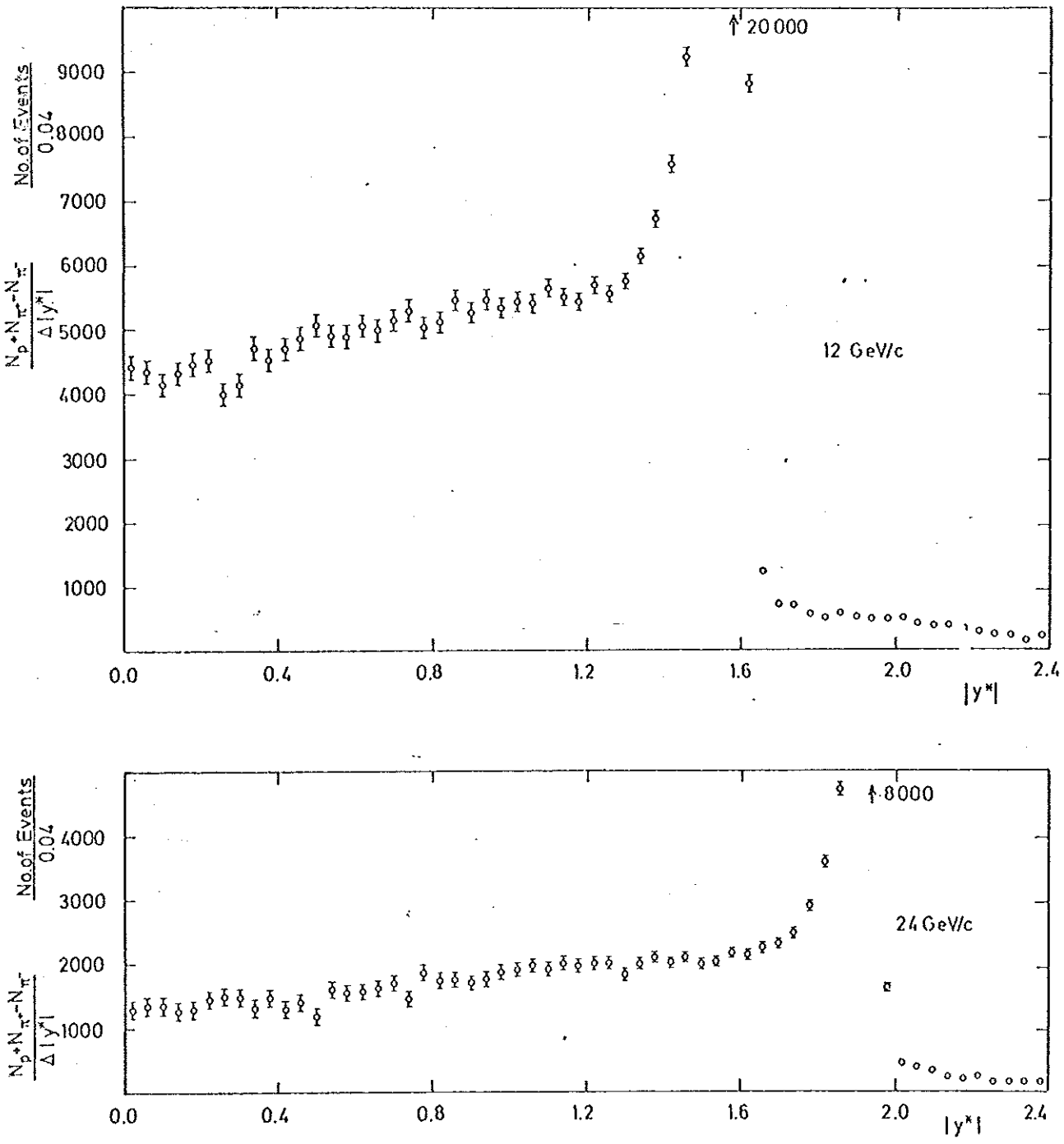
↑ 20 000
No. of Events / 0.04
$\frac{N_p+N_{\pi^+}-N_{\pi^-}}{\Delta|y^*|}$
9000
8000
7000
6000
5000
4000
3000
2000
1000
12 GeV/c
0.0
0.4
0.8
1.2
1.6
2.0
2.4
$|y^*|$
↑ 8000
No. of Events / 0.04
$\frac{N_p+N_{\pi^+}-N_{\pi^-}}{\Delta|y^*|}$
4000
3000
2000
1000
24 GeV/c
0.0
0.4
0.8
1.2
1.6
2.0
2.4
$|y^*|$

Fig. 4

Erratum:

Fig.2 of part II has been drawn wrongly. Below is the correct figure 2.

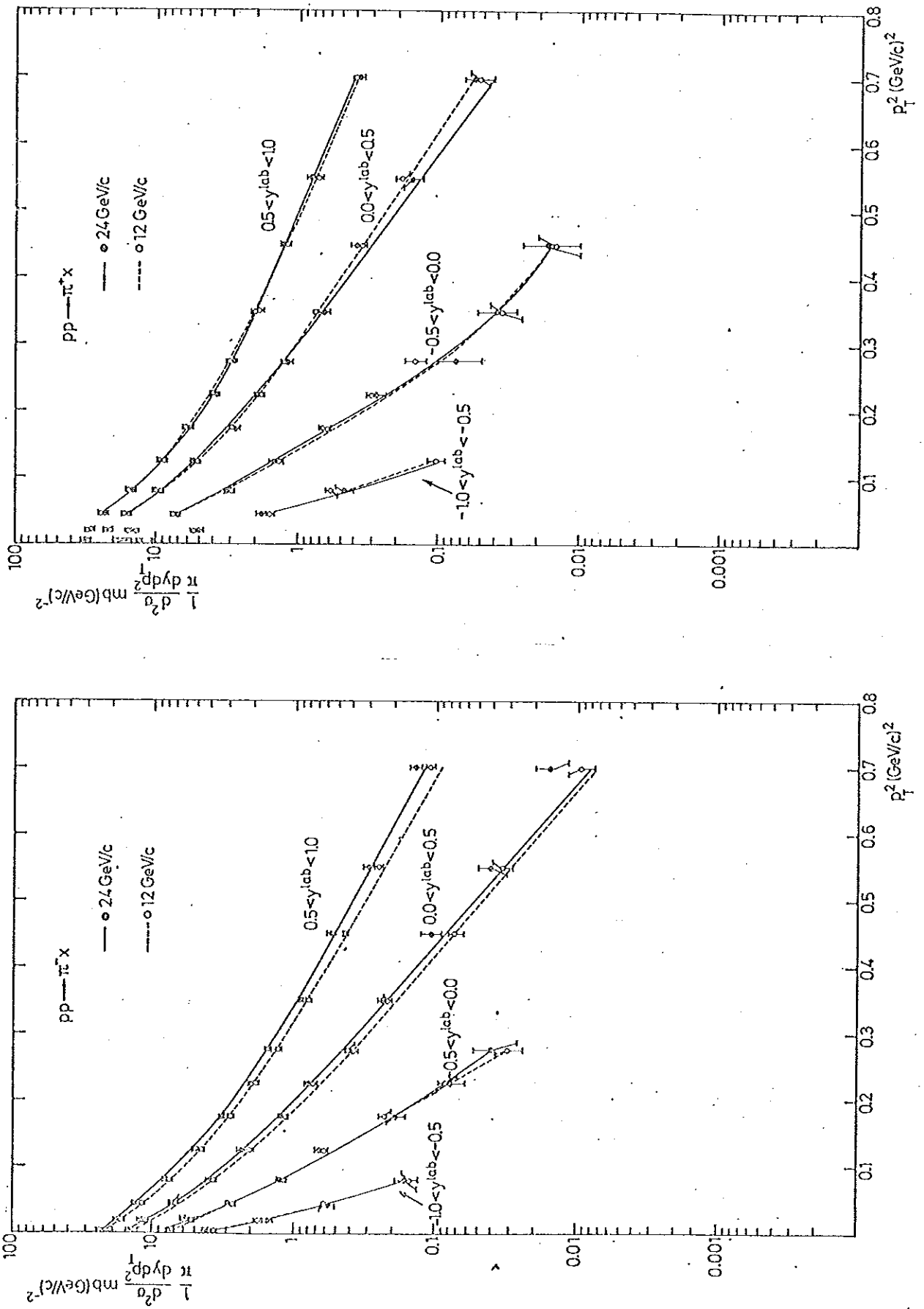

Fig. 2

Inclusive Particle Production in pp Interactions at 12 and 24 GeV/c; II. The Proton Fragmentation Region

H.J. Mück, M. Schachter, F. Selonke, and B. Wessels, University of Bonn;

V. Blobel, A. Brandt, H. Fesefeldt, B. Hellwig, D. Mönkemeyer, and H.F. Neumann, DESY and University of Hamburg;

G.W. Brandenburg*, H. Franz, W. Richter, W. Schrankel, B.M. Schwarzschild, and P. Weisbach, Max-Planck-Institut für Physik und Astrophysik, München

---

* Present address: Stanford Linear Accelerator Center, Stanford, California

In this contribution we present data[1] on the production of $\pi^{\pm}$, K^{o}_{s}, p, and Λ in inclusive reactions in the proton fragmentation region[2], and discuss their scaling behavior[3,4]. The invariant spectra $\frac{d^3\sigma}{d^3\vec{p}/E}$ are presented in double-differential form as functions of y^{lab} and p_T^2, and of x and p_T^2 for pions and protons; and in single-differential form, integrated over y^{lab} or p_T^2, for K^{o}_{s} and Λ. Here y^{lab} is the longitudinal rapidity in the laboratory system, x is Feynman's c.m.s. scaling variable, and p_T the transverse momentum. The $\pi^{\pm}$ and p spectra are compared with data on pp reactions obtained at the CERN Intersecting Storage Rings at laboratory equivalent momenta between 225 and 1500 GeV/c; the $\pi^{\pm}$ and Λ spectra are also compared with data from $\pi^{\pm}$p and K^{+}p bubble chamber experiments.

Our main conclusions on the invariant single-particle differential spectra as a function of y^{lab}, p_T^2 and s, in the proton fragmentation region, are the following:

p+p → π^{-}+X (Figs.1a,2a): The distribution is essentially s-independent for $y^{lab} < 0,5$ but increases when going from 12 to 24 GeV/c at the larger values of y^{lab}. Except for the lowest p_T and $y^{lab} > 0.8$, the ISR cross sections agree with our 24 GeV/c cross section.

p+p → π^{+}+X (Figs.1b,2b): The spectrum appears in general to be s-independent within about 20 % for $y^{lab} \lesssim 2$, from 12 GeV/c up to ISR energies. However there are "local" exceptions, e.g. the region $y \sim -0.6$ at $p_T \sim 0.4$ GeV/c, where the cross section changes by ~50 % between 12 and 24 GeV/c, presumably due to the changing cross section for nucleon isobar production.

p+p → K^{o}_{s}+X (Fig.4): We observe an increase by ~50 % between 12 and 24 GeV/c in the fragmentation region ($y^{lab} < 1$), and by about a factor of 2 in the central region.

p+p → p+X (Figs.5,6): The spectrum decreases from 12 to 24 GeV/c by ~20 %, but within the experimental uncertainties the ISR data appear to agree with the 24 GeV/c data, when plotted as a function of x.

p+p → Λ+X (Fig.7): The spectrum increases by ~30 % at all y^{lab},

Dependence on the quantum numbers of the projectile: Comparison of our π^+, π^- and Λ spectra in the proton fragmentation region with data from other experiments using $\pi^\pm$ and K^+ as projectiles (fig. 8) suggests that the projectile dependence factorizes when the reactions are exotic.

The data we show come from 130 000 events (54 000 events) observed in the CERN 2m hydrogen bubble chamber which was exposed to a p beam of 12 GeV/c (24 GeV/c). Events of all topologies were measured on Flying Spot Digitizers. The FSD also gives ionization information thus enabling us to distinguish between different kinematically acceptable hypotheses in most cases. All negative particles except those with a visible K^-, Σ^- or Ξ^- decay were assumed to be pions. For the π^+ we used only the c.m. backward hemisphere, where the fraction of ambiguities with protons is 10 % (16 %) at 12 (24) GeV/c. Assuming that all positive tracks are either pions or protons, these ambiguities for the backward π^+ could be resolved on a statistical basis, exploiting the symmetry in the c.m. system. This procedure will be described in a future publication. The proton distribution was then obtained by subtraction of the known π^+ distribution. The distributions of the K^o_s and Λ (which includes the Λ from Σ^o decays) are corrected for neutral decays, and also contain a correction for loss of events with short decay length and decays outside of the bubble chamber.

In Fig. 1 we show, as curves, our π^- and π^+ inclusive cross sections $\pi^{-1} d^2\sigma/dy\, dp_T^2$ at 12 and 24 GeV/c as a function of the laboratory longitudinal rapidity $y^{lab} = \sinh^{-1}(p_\parallel^{lab}/(p_T^2 + m^2)^{1/2})$ for different fixed values of p_T. Note that at $y^{lab} = 0$ the laboratory momentum is purely transverse (i.e. longitudinal momentum $p_\parallel^{lab} = 0$), and at $y^{lab} = 1.62$ (1.97) for 12 (24) GeV/c beam momentum the c.m. momentum is purely transverse. The ISR data are shown as points with error bars[5,6,7]. Our measurements are distributed over all p_T; to obtain values at definite p_T in order to compare with the ISR data, we have fitted the p_T^2 distributions at fixed y^{lab} with an interpolation function $a \cdot \exp(bp_T^2 + cp_T^4)$ in small regions of p_T^2, and have taken the cross sections at fixed

p_T^2 from these fits. The p_T^2 distributions are shown in fig.2.† In order not to confuse the picture, the errors of our measurements are not shown on fig. 1; they can be seen from fig. 2. In addition to the statistical errors indicated there, we have a systematic error which we estimate to be 2 % for the π^- and ~5 % for the π^+ cross sections.

Both the π^+ and the π^- spectra of figs. 1 and 2 are found to be s-independent within about 20 % for $y^{lab} < 0$, i.e. for backward going pions, except that in the π^+ spectrum there seem to be local, energy-dependent structures (e.g. at $y \sim -0.2$, $p_T \sim 0.2$ GeV/c and $y \sim -0.6$, $p_T \sim 0.4$ GeV/c) which are presumably due to isobar production which decreases with increasing energy. The π^+ data continue to be nearly s-independent also at larger y^{lab}, essentially in the whole measured y^{lab} range which extends up to $y^{lab} = 2$. In contrast to this the π^- data show increasing s-dependence as y^{lab} approaches the central region, near the symmetry points where the c.m. momentum is purely transverse. However, the increase observed between the 24 GeV/c data and the ISR data is not much larger than that between 12 and 24 GeV/c.

The same data plotted against the Feynman scaling variable $x = p_\parallel^*/(\sqrt{s}/2)$ instead of y^{lab}, where $p_\parallel^*$ is the c.m. longitudinal momentum, are shown in fig. 3. For $x^2 >> (p_T^2 + m_\pi^2)/s$, the specification of x and p_T determines $p_\parallel^{lab}$ independent of s. So for large x and small p_T, fig. 3 exhibits about the same degree of limiting behavior as fig. 1. Elsewhere the y^{lab} plots exhibits a somewhat clearer approach to limiting behavior than the x plots, as one would expect for limiting fragmentation.

For K_s^o production we show in fig. 4 only the integrated distributions $\pi^{-1} d\sigma/dy$ and $\pi^{-1} d\sigma/dp_T^2$ from our 12 and 24 GeV/c data, because of the much smaller statistics. The data are still preliminary. There is a ~50 % increase of $\pi^{-1} d\sigma/dy$ with s in the fragmentation region ($y^{lab} < 1$), and a stronger increase, by about a factor of 2, in the central region of larger y^{lab}.

† The curves in fig. 2 are actually not those used to interpolate the p_T^2 distributions, but instead are functions of the form $a \cdot \exp(bp_T^2) + c \cdot \exp(dp_T^2)$. This form fits over a larger range of p_T^2, although the fit is not in all cases statistically satisfactory.

This is strongly reminiscent of the behavior of the π^- distributions, although the formation of a central plateau, corresponding to pionization, is not yet apparent in the K^o_s data. Figure 4 also shows the invariant x distribution, integrated over all p_T^2; here also limiting behavior is not observed.

The inclusive p spectra at 12 and 24 GeV/c (our experiment, shown as curves) and at ISR energies (shown as points with errors)[7] are plotted against y^{lab} in fig. 5, and against x in fig. 6. The regions near $y^{lab} = 0$ or $x = -1$ (p at rest in the laboratory system) are not shown in the left-hand part of fig. 5 and in fig.6, since there the spectrum peaks strongly due to diffractive scattering. Transverse momentum distributions are also shown in fig.5. Both the y^{lab} and x distributions show a valley in the central region (near $y^{lab} = 1.62$ or 1.97 at 12 and 24 GeV/c respectively, corresponding to $x = 0$), which seems to become deeper with increasing s. In contrast to this, when we plot the non-invariant distribution $d^3\sigma/d^3\vec{p}$ we find it to be more nearly flat in the whole region of $|x| < 0.5$.

Our inclusive Λ spectra, which are still preliminary, are shown as a function of y^{lab} and x in fig. 7. We have defined x in this case by $x = p^*_{\parallel}/\text{Max } p^*_{\parallel}$, where Max $p^*_{\parallel}$ is the maximum longitudinal c.m. momentum kinematically possible for a Λ. With this definition $x = 1$ always is the kinematic limit, independent of s. Both the y^{lab} and the x distributions show some increase from 12 to 24 GeV/c. The transverse momentum distribution of the Λ's in the region $0 < y^{lab} < 1.62$ is also shown in fig. 7; one sees that the form of the p_T^2 dependence is nearly independent of s in a fixed region of y^{lab}. Note also the development of a similar dip in the y^{lab} and x distributions near the center ($x = 0$), as was already observed for the protons in figs. 5 and 6.

Finally we investigate whether the single-particle distributions in the proton target fragmentation region are independent of the quantum numbers of the projectile or, equivalently,

whether the (presumable pomeron-dominated) exchange factorizes. We therefore compare in fig. 8 our $\pi^{\pm}$ and Λ spectra from 12 and 24 GeV/c pp interactions with the published spectra from π^+p, π^-p and K^+p interactions at comparable incident momenta[8-11]. For the comparison we have scaled our pp data, which are shown as curves, by the ratio of the pomeron couplings to the beam particle, i.e. with $\sigma_T^{\infty}(K^+p)/\sigma_T^{\infty}(pp) \approx 0.446$ and $\sigma_T^{\infty}(\pi^{\pm}p)/\sigma_T^{\infty}(pp) \approx 0.615$, respectivley. The plotted invariant cross sections $d^3\sigma/(d^3\vec{p}/E)$ are integrated over $\vec{p}_T$. The abscissa variables had to be chosen in accord with the published plots from the other experiments; therefore we use here the different longitudinal variables y^{lab}, $p_{\parallel}^{lab}$ and x.

In Figures 8a,b,c and f the reactions compared with our data are, in the sense of Chan et al.[12], exotic as are our $\pi^{\pm}$ and Λ reactions. In these cases the overall agreement in the proton fragmentation region is seen to be reasonably good. An exception are the two points in fig. 8c at small p_T and large $|x|$ from the 11.8 GeV/c K^+p experiment[8] which, if true, indicate a very strong deviation from factorization. We remark however that this discrepancy occurs in a region of quite small cross sections, so that even a small experimental bias or background may have a relatively large effect. One should also point out that for $p_T < 0.2$ GeV/c the $K^+p \to \pi^-X$ data[8] (fig.8c) show distinctly more concavity than the $pp \to \pi^-X$ data. This is perhaps a departure from factorization. On the other hand, the less convincing comparison in fig. 8b [10] should be viewed in conjunction with fig. 8a [9] where good agreement is seen with the same reaction.

Figures 8d and e show the comparison of some non-exotic reactions with our scaled pp data. The $\pi^-p \to \pi^-X$ data to 18.5 GeV/c[9] (fig. 8d) are still quite far above our $pp \to \pi^-X$ distribution; in fact Shephard et al.[9] point out that their non-exotic data (fig. 8d) tend towards their exotic spectrum (fig. 8a), and hence towards our $pp \to \pi^-X$ spectrum scaled (see fig. 8a), like $s^{-1/2}$ in the proton fragmentation region. It may

also be that at these energies the proton target fragmentation products are still not well separated kinematically from the projectile fragmentation products (whose π^-/π^+ ratio presumably is different for a π^- and a proton projectile). To a lesser degree, also the non-exotic $\pi^+ p \to \pi^+ X$ spectrum at 16 GeV/c [10] (fig. 8e) is found to lie above our $pp \to \pi^+ X$ data.

We are indebted to the CERN operation crews of the PS and of the 2m bubble chamber for their excellent cooperation. We wish to particularly thank H.H. Nagel and J. Seyerlein, who have been responsible for the development of our Flying-Spot Digitizers. Finally we thank E. Lohrmann, H.H. Nagel, N. Schmitz, P. Söding and M.W. Teucher for advice, help, criticism, and active support.

References

1. For published data on the same reactions at similar energies see the following references:
D.B. Smith, R.J. Sprafka and J.A. Anderson, Phys. Rev. Letters 23 (1969) 1064;
H. Bøggild, K.H. Hansen and M. Suk, Nuclear Physics B27 (1971) 1;
J.V. Allaby et al., Contribution to the Amsterdam International Conference on Elementary Particles 1971;
R.S. Panvini et al., Physics Letters 38 (1972) 55;
E.L. Berger, B.Y.Oh and G.A. Smith, Phys. Rev. Letters 28 (1972) 322.

2. Our results for the central or pionization region are presented in another paper, entitled "Inclusive Particle Production in pp Interactions at 12 and 24 GeV/c; I. The Central Region."

3. J. Benecke, T.T. Chou, C.N. Yang and E. Yen, Phys. Rev. 188 (1969) 2159.

4. R.P. Feynman, in High Energy Collisions (Ed. C.N. Yang et al.), New York 1969, p.237; Phys. Rev. Letters 23 (1969) 1415.

5. L.G. Ratner et al., Phys. Rev. Letters 27 (1971) 68, and to be published.

6. A. Bertin et al., Physics Letters 38 (1972) 260.

7. A. Krisch, private communication

8. W. Ko and R.L. Lander, Phys. Rev. Letters 26 (1971) 1064.

9. W.D. Shephard et al., Phys. Rev.. Letters 27 (1971) 1164; 28, 260(E) (1972); and private communication from V.P.Kenney.

10. J.V. Beaupre et al., Physics Letters 37 (1971) 432.

11. S. Stone et al., University of Rochester Preprint No. UR-875-349.

12. Chan Hong-Mo et al., Phys. Rev. Letters 26 (1971) 672.

Figure Captions

Fig. 1. Rapidity distributions of π^- and π^+.

Fig. 2. Transverse momentum distributions of π^- and π^+.

Fig. 3. Distributions of $x = 2\,p^*_{\parallel}/\sqrt{s}$ for π^- and π^+.

Fig. 4. Distribution of y^{lab}, x and p_T^2 for K^o_s (with $x = 2p^*_{\parallel}/\sqrt{s}$).

Fig. 5. Rapidity and transverse momentum distributions for protons.

Fig. 6. Distribution of $x = 2p^*_{\parallel}/\sqrt{s}$ for protons.

Fig. 7. y^{lab}, x and p_T^2 distributions for Λ (with $x = p^*_{\parallel}/\text{Max } p^*_{\parallel}$).

Fig. 8. Comparison of π^-, π^+ and Λ distributions from various other experiments[8-11] using $\pi^\pm$ or K^+ beams, with our data (with p beam). The p beam cross sections, multiplied by the ratio $\sigma^\infty_{\pi p}/\sigma^\infty_{pp}$ or $\sigma^\infty_{K^+p}/\sigma^\infty_{pp}$ respectively, are shown as curves.

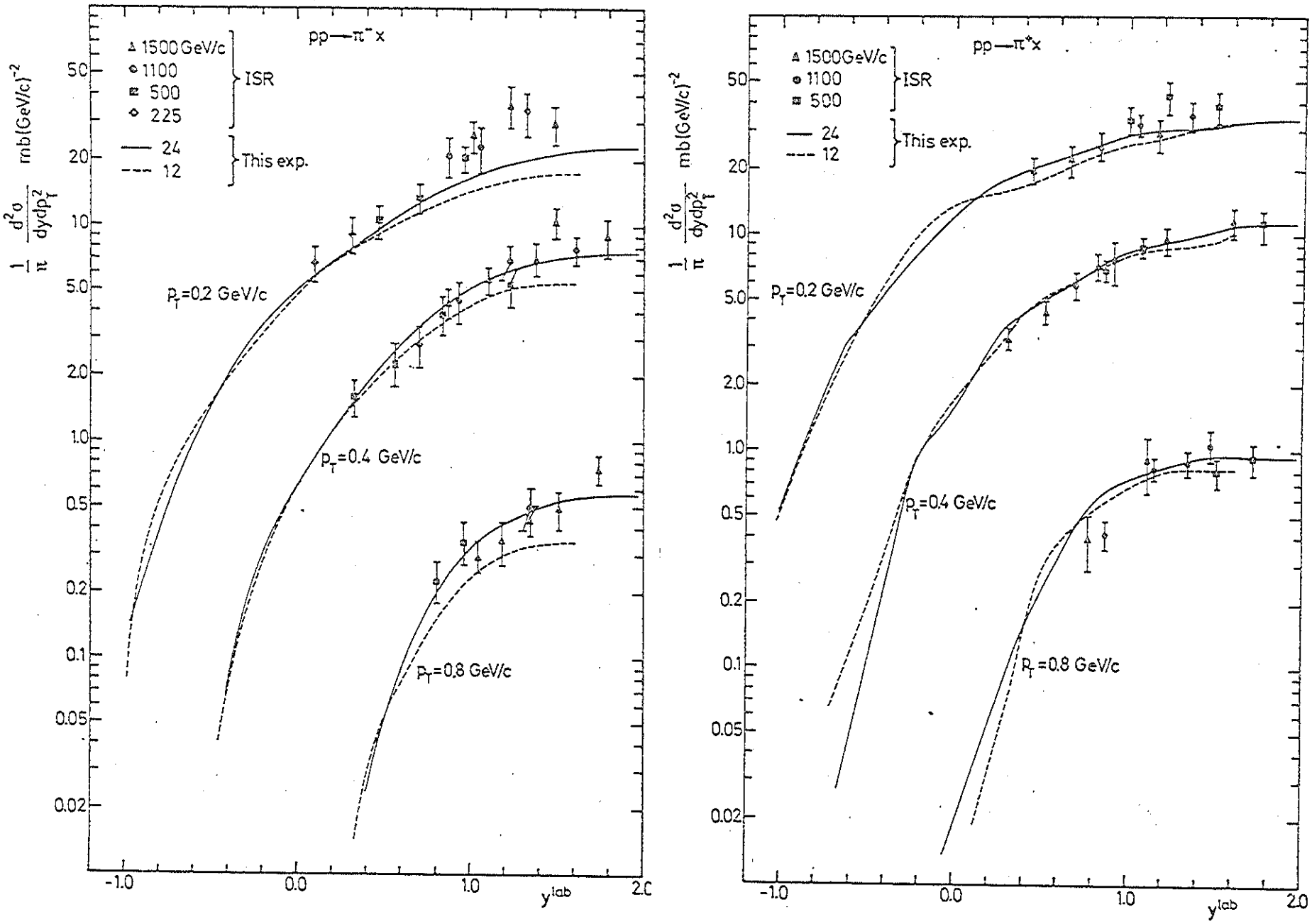
pp—π⁻x
1500 GeV/c
1100
500
225
ISR
24
12
This exp.
$\frac{1}{\pi}\frac{d^2\sigma}{dydp_T^2}$ mb(GeV/c)$^{-2}$
p_T=0.2 GeV/c
p_T=0.4 GeV/c
p_T=0.8 GeV/c
y^{lab}
pp—π⁺x
1500GeV/c
1100
500
ISR
24
12
This exp.
$\frac{1}{\pi}\frac{d^2\sigma}{dydp_T^2}$ mb(GeV/c)$^{-2}$
p_T=0.2 GeV/c
p_T=0.4 GeV/c
p_T=0.8 GeV/c
y^{lab}

Fig. 1

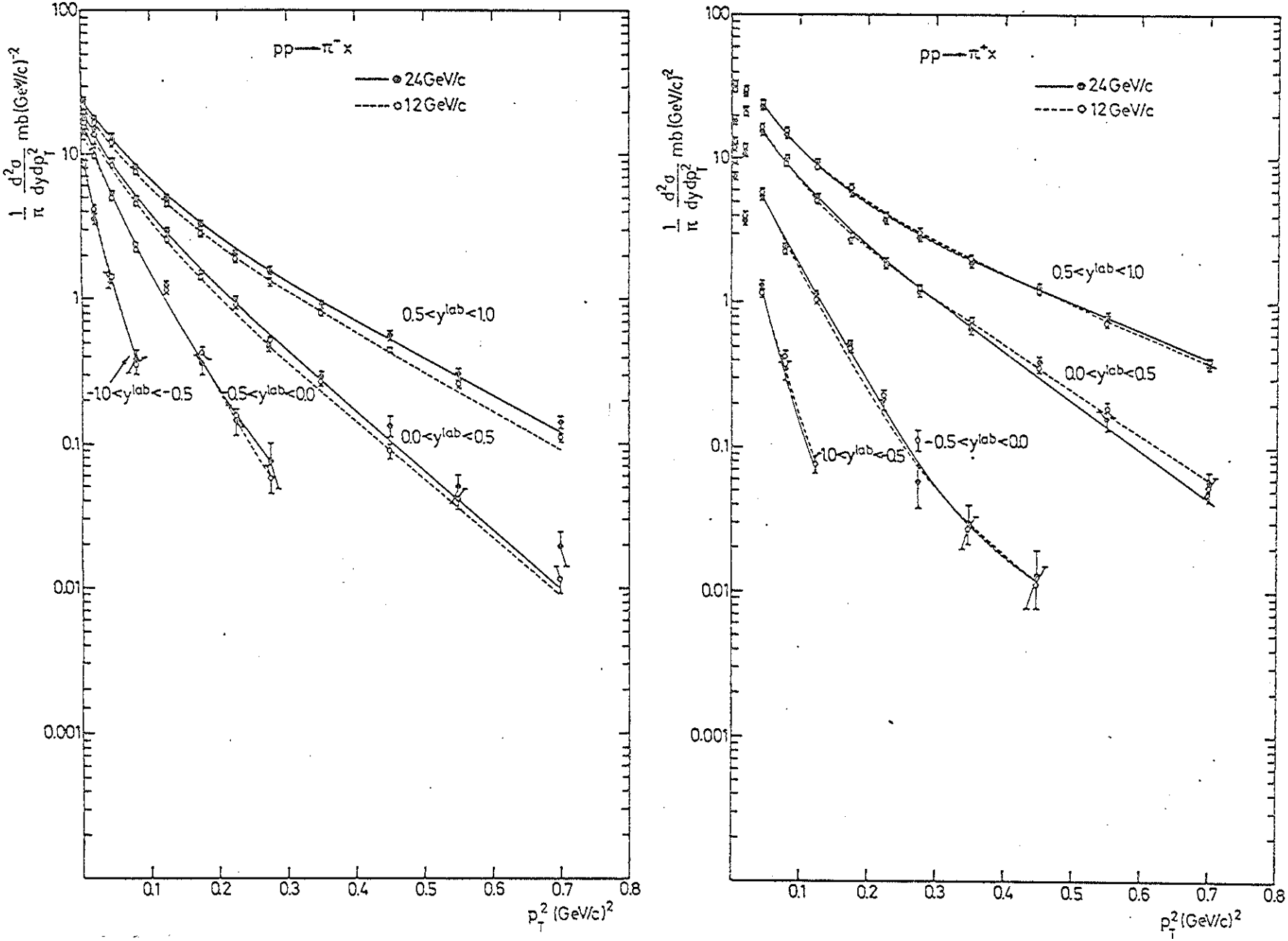
pp→π⁻x
24GeV/c
12GeV/c
0.5<y^lab<1.0
0.0<y^lab<0.5
-0.5<y^lab<0.0
-1.0<y^lab<-0.5
$\frac{1}{\pi}\frac{d^2\sigma}{dydp_T^2}$ mb(GeV/c)$^{-2}$
p_T^2 (GeV/c)^2
pp→π⁺x
24GeV/c
12GeV/c
0.5<y^lab<1.0
0.0<y^lab<0.5
-0.5<y^lab<0.0
-1.0<y^lab<-0.5
$\frac{1}{\pi}\frac{d^2\sigma}{dydp_T^2}$ mb(GeV/c)^2
p_T^2 (GeV/c)^2

Fig. 2

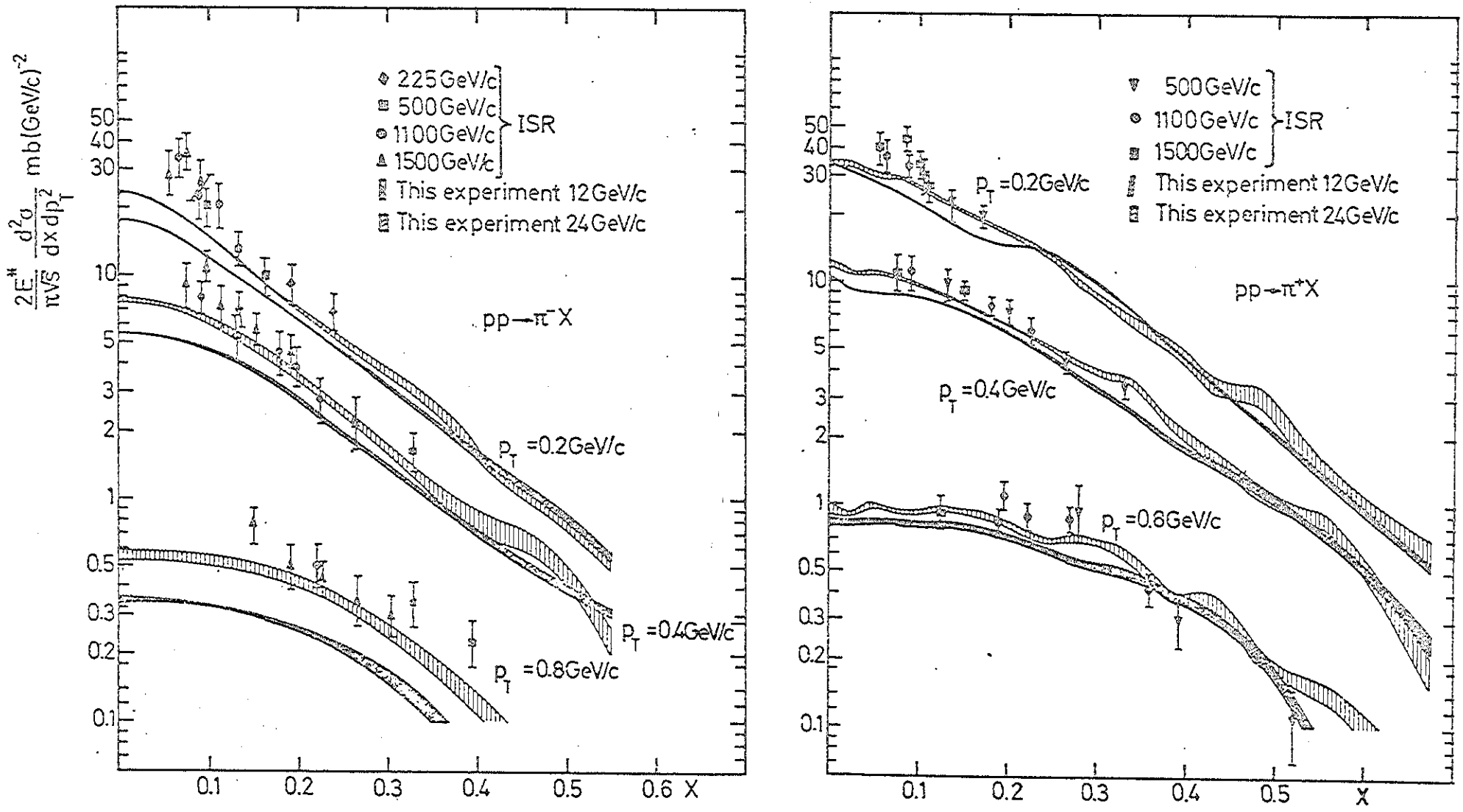
$\frac{2E^*}{\pi\sqrt{s}}\frac{d^2\sigma}{dx\,dp_T^2}$ mb(GeV/c)$^{-2}$
225 GeV/c
500 GeV/c
1100 GeV/c
1500 GeV/c
ISR
This experiment 12 GeV/c
This experiment 24 GeV/c
pp→π⁻X
p_T =0.2GeV/c
p_T =0.4GeV/c
p_T =0.8GeV/c
X
500 GeV/c
1100 GeV/c
1500 GeV/c
ISR
This experiment 12GeV/c
This experiment 24GeV/c
p_T =0.2GeV/c
pp→π⁺X
p_T =0.4GeV/c
p_T =0.6GeV/c
X

Fig. 3

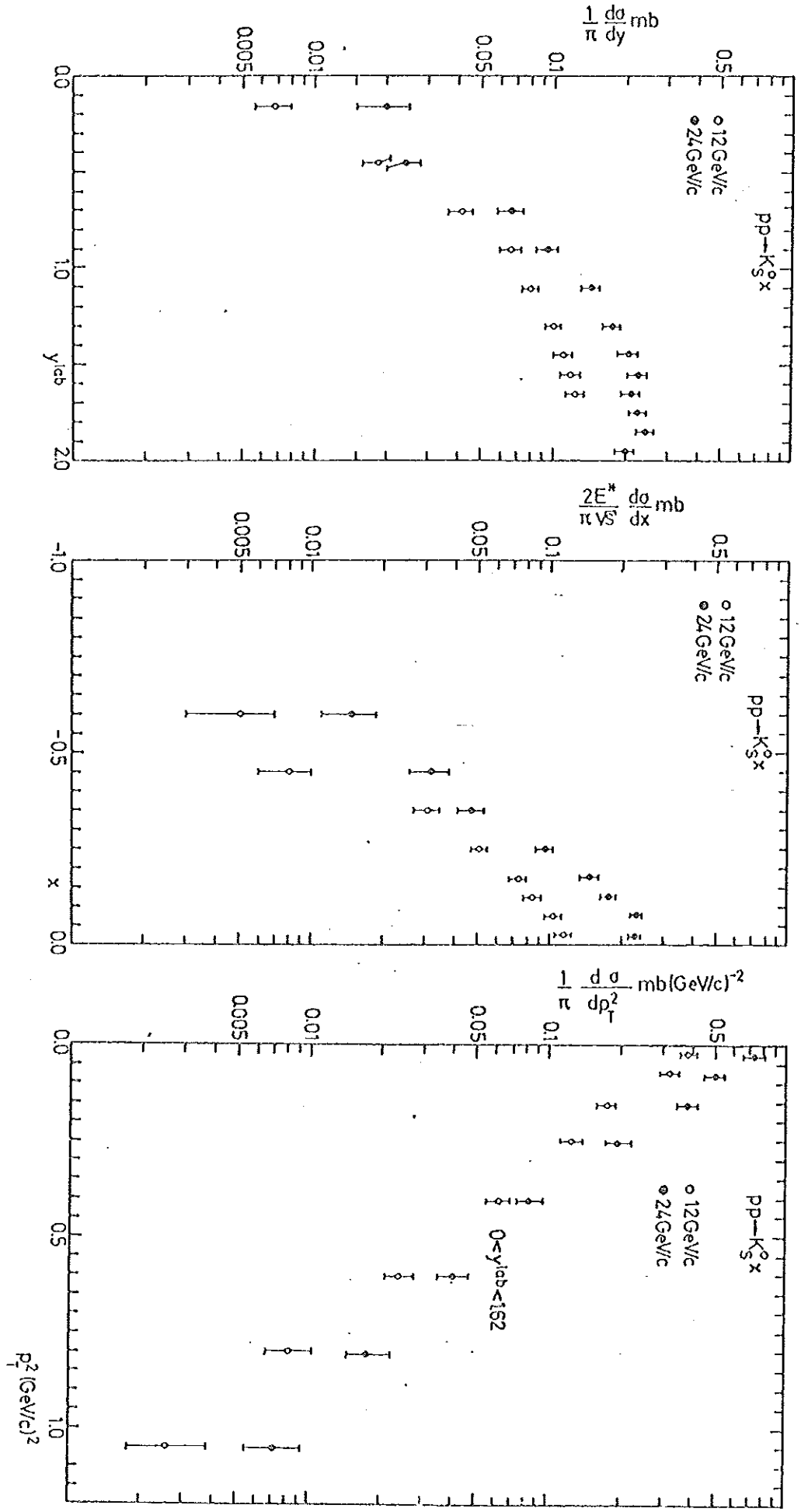
$\frac{1}{\pi}\frac{d\sigma}{dy}$ mb
0.005
0.01
0.05
0.1
0.5
0.0
1.0
2.0
y^{lab}
○ 12 GeV/c
● 24 GeV/c
pp→K^0_Sx
$\frac{2E^*}{\pi\sqrt{s}}\frac{d\sigma}{dx}$ mb
-1.0
-0.5
x
$\frac{1}{\pi}\frac{d\sigma}{dp_T^2}$ mb(GeV/c)$^{-2}$
p_T^2 (GeV/c)^2
0<y^{lab}<1.62

Fig. 4

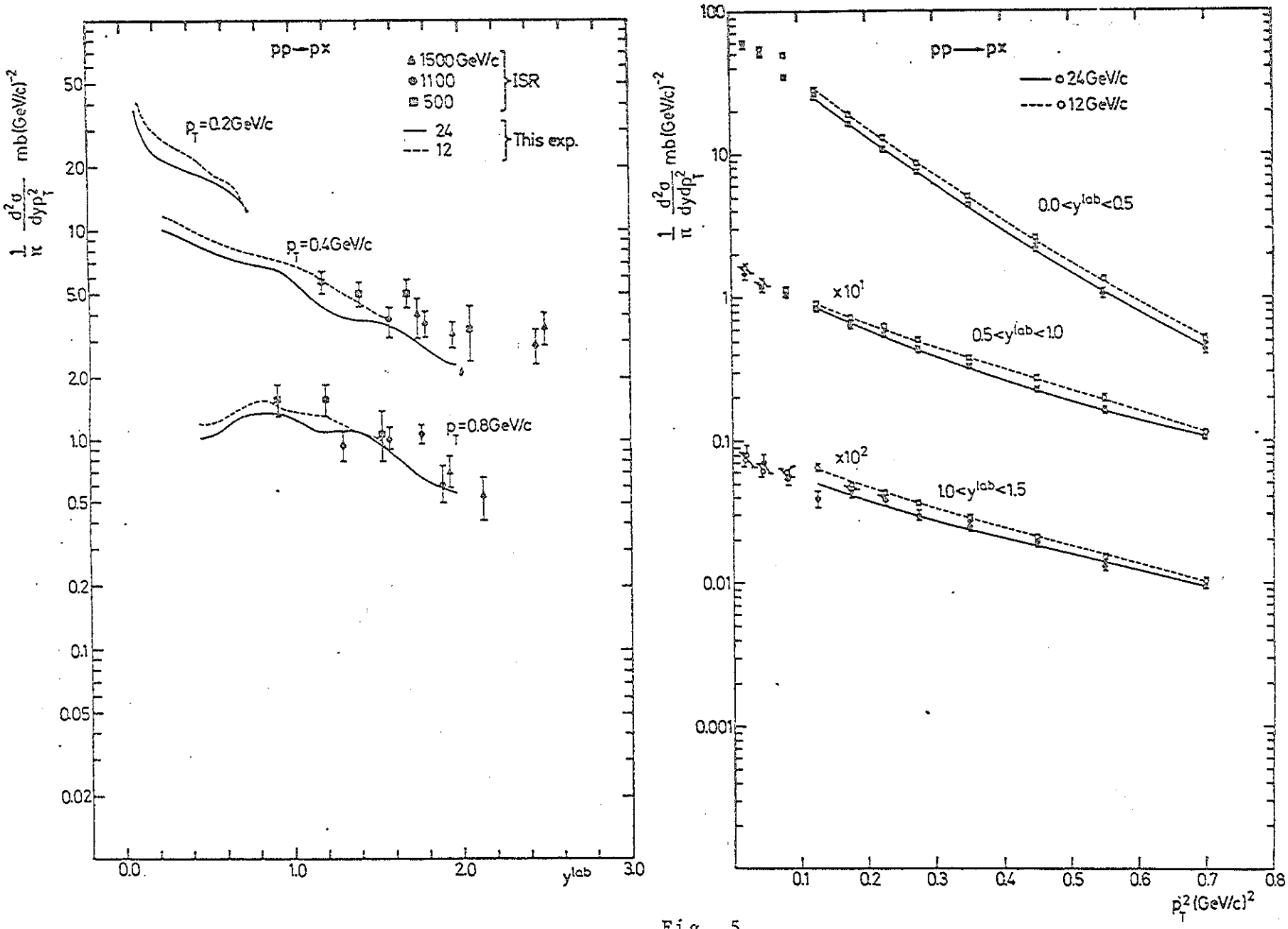
pp→px
△ 1500 GeV/c
○ 1100
□ 500
ISR
— 24
--- 12
This exp.
p_T=0.2GeV/c
p_T=0.4GeV/c
p_T=0.8GeV/c
$\frac{1}{\pi}\frac{d^2\sigma}{dyp_T^2}$ mb(GeV/c)$^{-2}$
y^{lab}
pp→px
o 24GeV/c
o 12GeV/c
0.0<y^{lab}<0.5
×10^1
0.5<y^{lab}<1.0
×10^2
1.0<y^{lab}<1.5
p_T^2 (GeV/c)^2

Fig. 5

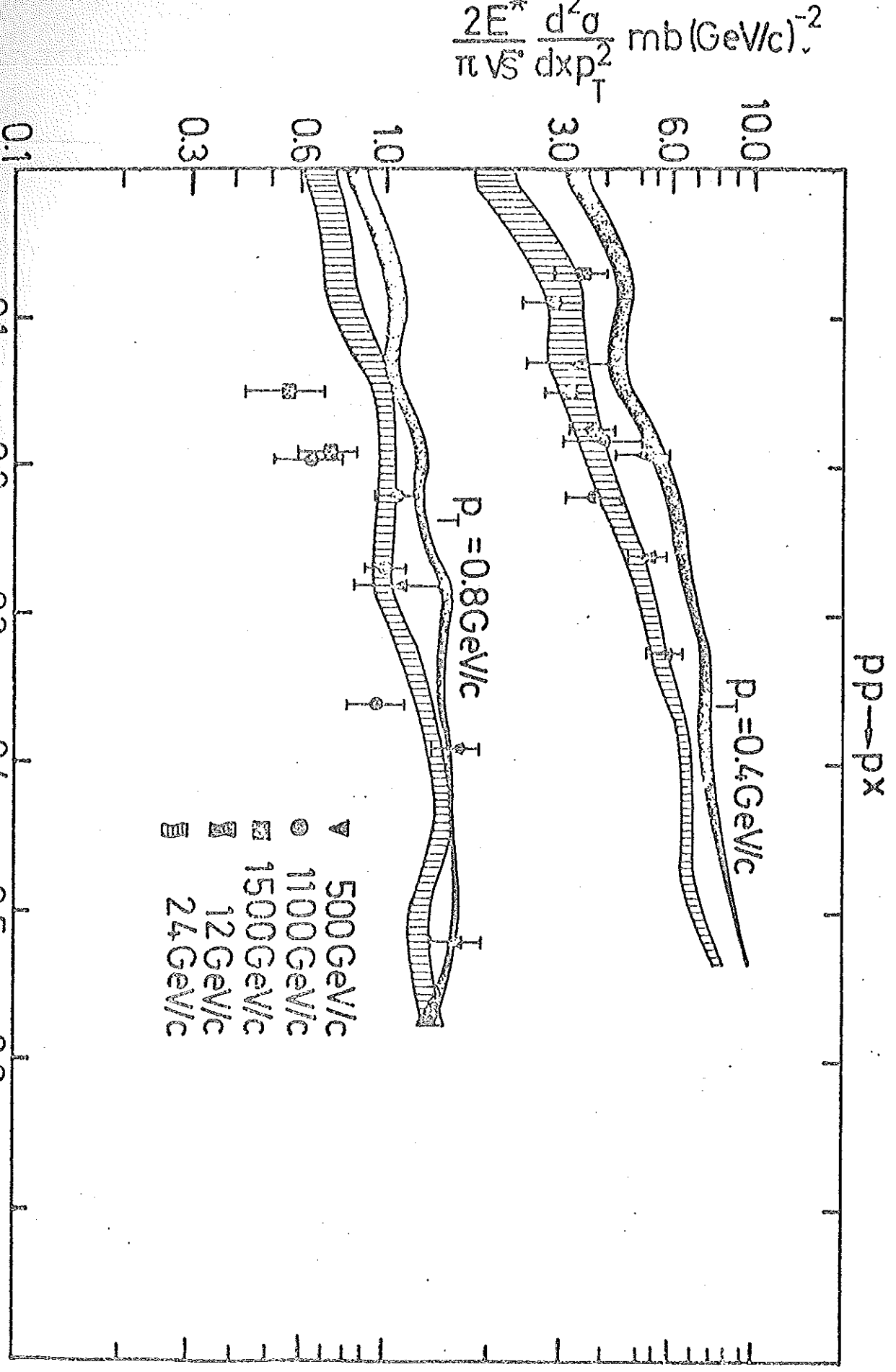
$\frac{2E^*}{\pi\sqrt{s}}\frac{d^2\sigma}{dxp_T^2}$ mb(GeV/c)$^{-2}$
0.1
0.3
0.6
1.0
3.0
6.0
10.0
0.1
0.2
0.3
0.4
0.5
0.6
x
p_T=0.8GeV/c
p_T=0.4GeV/c
500GeV/c
1100GeV/c
1500GeV/c
12GeV/c
27GeV/c
pp→px

Fig. 6

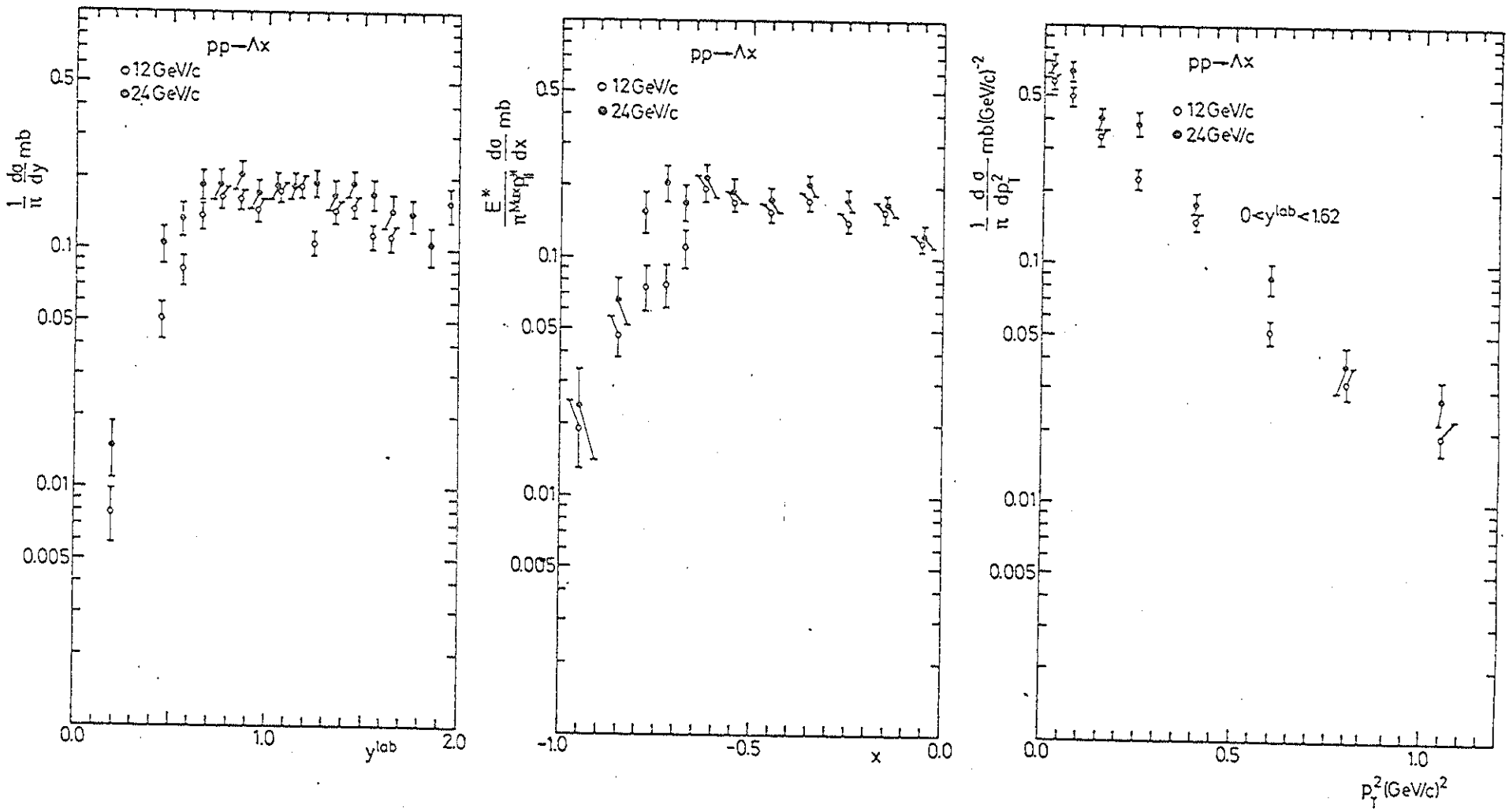
pp—Λx
○ 12 GeV/c
● 24 GeV/c
$\frac{1}{\pi}\frac{d\sigma}{dy}$ mb
y^{lab}
$\frac{E^*}{\pi^{Max}p_{\parallel}^*}\frac{d\sigma}{dx}$ mb
x
$\frac{1}{\pi}\frac{d\sigma}{dp_T^2}$ mb(GeV/c)$^{-2}$
$0<y^{lab}<1.62$
p_T^2(GeV/c)^2

Fig. 7

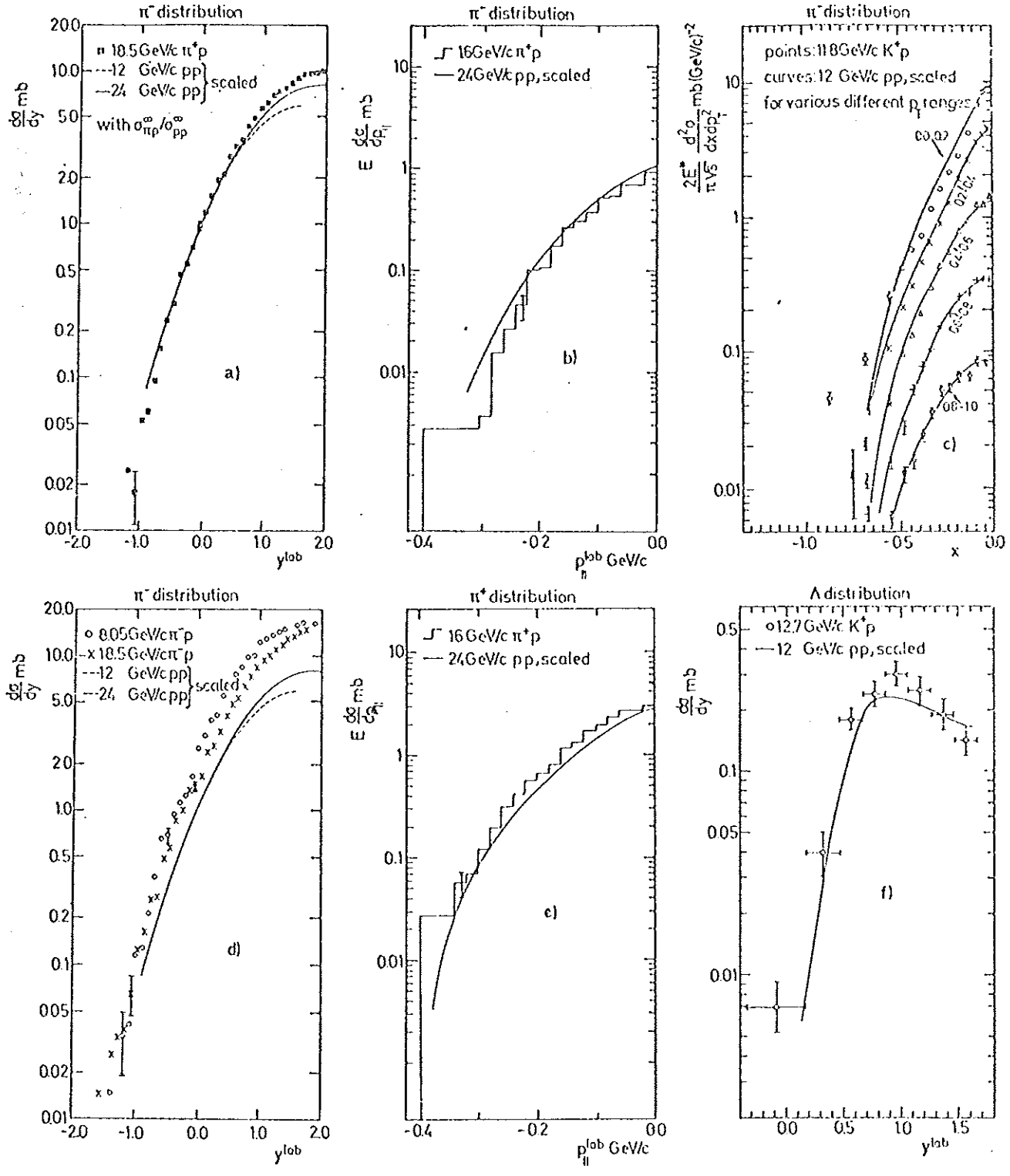
π⁻ distribution
π 18.5 GeV/c π⁺p
12 GeV/c pp
24 GeV/c pp
scaled
with σ^∞_πp/σ^∞_pp
a)
y^lab
π⁻ distribution
16 GeV/c π⁺p
24 GeV/c pp, scaled
b)
p^lab_π GeV/c
π⁻ distribution
points: 11.8 GeV/c K⁺p
curves: 12 GeV/c pp, scaled
for various different p_T ranges
c)
x
π⁻ distribution
8.05 GeV/c π⁻p
18.5 GeV/c π⁻p
12 GeV/c pp
24 GeV/c pp
scaled
d)
y^lab
π⁺ distribution
16 GeV/c π⁺p
24 GeV/c pp, scaled
e)
p^lab_π GeV/c
Λ distribution
12.7 GeV/c K⁺p
12 GeV/c pp, scaled
f)
y^lab

Fig. 8